THE ASTROPHYSICAL JOURNAL, 354:242–246, 1990 May 1

INFRARED IMAGES OF IONIZED AND MOLECULAR HYDROGEN EMISSION IN S106

SAEKO S. HAYASHI,[1] TETSUO HASEGAWA,[2,3] MASUO TANAKA,[2,3] MASAHIKO HAYASHI,[4] COLIN ASPIN,[5]
IAN S. MCLEAN,[5] PETER W. J. L. BRAND,[6] AND IAN GATLEY[7]
Received 1989 March 9; accepted 1989 November 6

ABSTRACT

We present high-resolution emission-line images of the central arcminute of S106 in Brγ and H_2 $v = 1$–0 $S(1)$. The images were taken at UKIRT through a Fabry-Perot filter of 130 km s^{-1} resolution using the infrared array camera IRCAM with a pixel size of 0.″62. The Brγ emission shows a clear bipolar distribution which resembles that of the radio continuum emission. The central dark lane caused by the disk is wider in the Brγ image than in comparable radio continuum images. The molecular hydrogen emission is predicted to originate in the dynamically shocked regions and/or in the photodissociation regions formed at the interface between the H II region and the clumpy molecular gas. For the case of S106, the peaks of the H_2 emission are located $\sim 5''$ outside the corresponding Brγ peaks; that is, further from the central star. The assumption that this displacement corresponds to the typical depth of the H_2 emitting zone in the photodissociation region, at which $A_v \simeq 2$ mag, leads to a density estimate of $\sim 10^5$ cm^{-3}.

This high density, together with the low excitation temperature reported earlier for S106, suggests that the origin of the *thermal* component in the H_2 emission measured by Tanaka *et al.* is either *high-density fluorescence*, that is, collisional de-excitation of the UV pumped H_2 in photodissociation regions formed on the dense molecular clumps beyond the ionization fronts, or it is radiation from *slow shocks* driven by the wind from the central source, propagating into the dense clumps. In either case, a novel physical environment is required to understand the observations.

Subject headings: interstellar: molecules — nebulae: H II regions — nebulae: individual (S106) — stars: formation

I. INTRODUCTION

Vibrationally excited molecular hydrogen is often found in the vicinity of young stellar objects. Such emission was invariably interpreted in terms of thermal excitation in dynamical shocks (e.g., Beckwith *et al.* 1978) until recent excitation studies revealed the presence of fluorescent emission from radiatively excited molecular hydrogen (e.g., Hayashi *et al.* 1985; Gatley *et al.* 1987, hereafter Paper I; Hasegawa *et al.* 1987, hereafter Paper II). In practice, molecular hydrogen emission is generally found to be a mixture of thermal and fluorescent emission whose ratio varies from one source to another (Tanaka *et al.* 1989, hereafter Paper III). Theoretical calculations suggest that the radiatively excited molecular hydrogen exists in thin ($A_v \leq 2$ mag) layers in photodissociation regions (PDR) (Tielens and Hollenbach 1985), but there are, as yet, no observations of sufficiently high spatial resolution to display structural details of PDRs.

S106 is a bipolar H II region with a young massive star at the center. The distance is estimated to be 600 pc (Staude *et al.* 1982). The central star, which we will refer to as S106IR, has a bolometric luminosity of 2×10^4 $L_\odot$ (Harvey *et al.* 1982), corresponding to a zero-age main sequence star of spectral type late O or early B. The bipolar H II region is separated by a narrow gap, which is seen even in radio continuum images, suggesting that an almost edge-on disk still exists around the central star (e.g., optical/infrared: Gehrz *et al.* 1982; Hodapp and Becklin 1988; Aspin *et al.* 1989*a*; radio: Bally, Snell, and Predmore 1983; Felli *et al.* 1984). The molecular/dust disk is also reported at various scale sizes (e.g., Bally and Scoville 1982; Bieging 1984; Harvey, Lester, and Joy 1987; Mezger *et al.* 1987; Kaifu and Hayashi 1987). Two micron polarimetric observations have shown an extended reflection nebula of $\sim 3'$ radius, illuminated by S106IR (McLean *et al.* 1987), demonstrating directly that a large neutral envelope surrounds the ionized cavity delineated by the optical and radio continuum images. A ridge of molecular hydrogen emission has been found in this neutral envelope (Longmore, Robson, and Jameson 1986); its relationship with the H II region is not clearly understood.

In this paper, we present high-resolution images of H_2 $v = 1$–0 $S(1)$ and Brγ emission from S106 obtained with the infrared camera at UKIRT, which clearly show that the H_2 emission is located just outside the H II region.

II. OBSERVATIONS

The observations of Brγ ($\lambda = 2.166$ μm) and H_2 $v = 1$–0 $S(1)$ ($\lambda = 2.122$ μm) were made in 1987 August with the infrared array system IRCAM on the 3.8 m United Kingdom Infrared Telescope, Mauna Kea, Hawaii. The array used was a Santa Barbara Research Center 62 × 58 InSb device, cooled to 35 K. For detailed specifications of the instrument and the data acquisition, see McLean *et al.* (1986), McLean (1989), and Aspin *et al.* (1988). The pixel-defined spatial resolution was 0.″62. A Fabry-Perot etalon manufactured by Queensgate Instruments was placed in front of the camera window and gave a spectral resolution (FWHM) of 130 km s^{-1}. A cold wide-band K filter in series with a cold narrow-band Brγ or H_2 $v = 1$–0 $S(1)$ line filter was used to specify the passband and to

[1] James Clerk Maxwell Telescope, Joint Astronomy Centre.
[2] Nobeyama Radio Observatory.
[3] Institute of Astronomy, University of Tokyo.
[4] Department of Astronomy, University of Tokyo.
[5] United Kingdom Infrared Telescope, Joint Astronomy Centre.
[6] Department of Astronomy, University of Edinburgh.
[7] National Optical Astronomy Observatories.

minimize the background radiation falling on the detector. The planetary nebula NGC 7027, which shows strong emission in both Brγ and H_2 lines, was used to tune the setting of the spectrometer. The fluxes of the current data are estimated using our NGC 7027 frames adopting the published line strengths for Brγ (Merrill, Soifer, and Russell 1975; Smith, Larson, and Fink 1981) and H_2 $v = 1$–0 $S(1)$ (Smith, Larson, and Fink 1981; Longmore, Robson, and Jameson 1986). The tracking of the telescope was adjusted by monitoring the optical image of S106 itself on a TV monitor. In addition, during the off-line data analysis, the infrared images were reregistered with respect to the strong point source S106IR.

Each image in the H_2 line is constructed from a set of four observations, taken at frequencies on and off the line and at positions on and off the source. That is, the data are both *frequency-switched* and *position-switched*. Five on-source spatial positions were measured in each line: one frame centered on S106IR and four others each offset by 15″ in both right ascension and declination. These five frames have been registered with reference to S106IR apparent in all frames before the sky subtraction and then been combined into a single image of 1 arcmin^2. The positional error caused in this registration process is mainly due to the identification of the centroid of S106IR and is not more than 1 pixel. Bright clumps and filaments are also used in supplement to assist the positioning. For the *off-line* wavelength, the Fabry-Perot filter was set 0.0027 μm shorter than the *on-line*. This difference, 0.13% in the wavelength, is sufficiently close to the maximum transmission within a narrow-band filter of 1% width. The observational sequence for Brγ was the same as that for H_2 except that only the frequency switch mode was used, and no sky frame was subtracted; the signal-to-noise ratio and the flatness are ample for the comparison with H_2 data. The total exposure times for Brγ and H_2 data were 1 minute and 7 minutes, respectively.

III. RESULTS

The Brγ image in the top left panel of Figure 1 (Plate 10) shows a clear bipolar distribution as seen in the radio continuum (e.g., Bally, Snell, and Predmore 1983; Felli *et al.* 1984). The central dark lane caused by a dust disk appears wider in the Brγ image than in the radio continuum because of the extinction in Brγ. The slight tilt of this almost edge-on disk causes more obscuration in the northern lobe. Note that the velocity field of the ionized gas is bipolar, with a receding northern lobe and an approaching southern lobe, as observed in optical line spectroscopy (Solf and Carsenty 1982). Limb brightening in the southern lobe indicates that the Brγ emission arises from a shell, not from a filled cone.

Most of the bright clumps and ridges coincide with IR sources detected at 10 and 20 μm by Gehrz *et al.* (1982). The brightest feature in the southwest corresponds to IRS 3. The spatial coincidence of the ionized clumps and the 10 and 20 μm emission is a subsidiary supporting case for the interpretation of Gehrz *et al.* (1982) that the infrared emission comes from warm dust associated with the ionization fronts.

The total flux of Brγ in S106 over the observed area is estimated to be $5(\pm 1) \times 10^{-18}$ W cm^{-2}. This uncertainty is introduced by the sky level in the current measurement and by the scatter of the measured flux of NGC 7027 in the literature. Our adopted calibration gives a flux for S106IR of about 5×10^{-19} W cm^{-2}, which agrees well with previous aperture photometry (Felli *et al.* 1984; Persson *et al.* 1984). The fluxes of the northern and southern lobes are 40% and 60% of the total Brγ emission, respectively. This is caused by the difference in the foreground extinction; typically $A_v = 12$ mag toward the northern lobe and 8 mag toward the southern lobe (Felli *et al.* 1984). The total flux of Brγ corrected for foreground extinction is $1.1(\pm 0.2) \times 10^{-17}$ W cm^{-2}.

While the Brγ image shows the familiar structure of the ionized bipolar lobes, the H_2 image resolved fine structures within the ridge known from the measurement by Longmore, Robson, and Jameson (1986). The molecular hydrogen emission, shown in the upper right panel of Figure 1, remains bipolar as a whole—separated to the north and south by the central dark lane—but the region occupied by the H_2 emission is wider in the east-west direction than the Brγ emission. The eastern and western ridges are equally bright in H_2, but the western region is brighter in Brγ. The bright H_2 emission comes from several clumps and filaments. The surface brightness of these H_2 clumps is typically 1–2 $\times 10^{-4}$ ergs s^{-1} cm^{-2} sr^{-1}, which is 5–10 times brighter than the interclump region.

The most conspicuous difference between the distribution of Brγ and vibrationally excited H_2 emission is that the H_2 originates slightly farther from S106IR. Each clump is seen in both Brγ and H_2 with an almost perfect one-to-one correspondence, but the peaks of H_2 are located just outside the Brγ by 3″–7″, as shown in Figure 2 (Plate 11). These offsets are definitely larger than the positional uncertainties of the H_2 and Brγ images (see § II). We interpret this displacement as a direct measure of the density of the clumps (see § IV).

The total flux of H_2 $v = 1$–0 $S(1)$ for the observed area of S106 is estimated to be about $4(\pm 1) \times 10^{-19}$ W cm^{-2}. This uncertainty is mainly due to that in the sky level. The measured flux corresponds to half of that measured by Longmore, Robson, and Jameson (1986) which includes the diffuse emission extending beyond the boundaries of the current 1′ frame. In contrast to the Brγ flux, the H_2 flux in the northern lobe is 1.3 times brighter than that in the southern lobe in the raw data; after the extinction correction for foreground material, using the same values of A_v as for the Brγ flux, the flux of the northern lobe is 1.8 times that of the southern lobe. The total flux after this correction is $9(\pm 3) \times 10^{-19}$ W cm^{-2}. This H_2 flux imbalance between the north and south suggests some variation in the properties in the neutral envelope—probably in its density and clumpiness.

The bottom left panel of Figure 1 shows the distribution of the diffuse 2 μm continuum emission, which is more uniform than the Brγ and the H_2 emission, especially in the northern lobe. This is probably a consequence of scattering by dust. Polarization measurements with a 20″ aperture by McLean *et al.* (1987) show that an infrared reflection nebula extends out to 3′ from S106IR. In the inner region of the nebulosity, the radiation may be a mixture of the scattered light (Aspin *et al.* 1989*a*, *b*) and emission from transiently heated very small grains (e.g., Sellgren, Werner, and Dinerstein 1982).

IV. DISCUSSION

The peaks of the H_2 emission observed throughout S106 are located 3″–7″ (that is, 3–6 $\times 10^{16}$ cm) farther from the central star than the corresponding Brγ peaks, a situation reminiscent of that found in the Orion bright bar, where the H_2 emission peaks $\sim$30″ (2×10^{17} cm) farther from the Trapezium stars than the ionized gas emission (Hayashi *et al.* 1985). The overall

PLATE 10

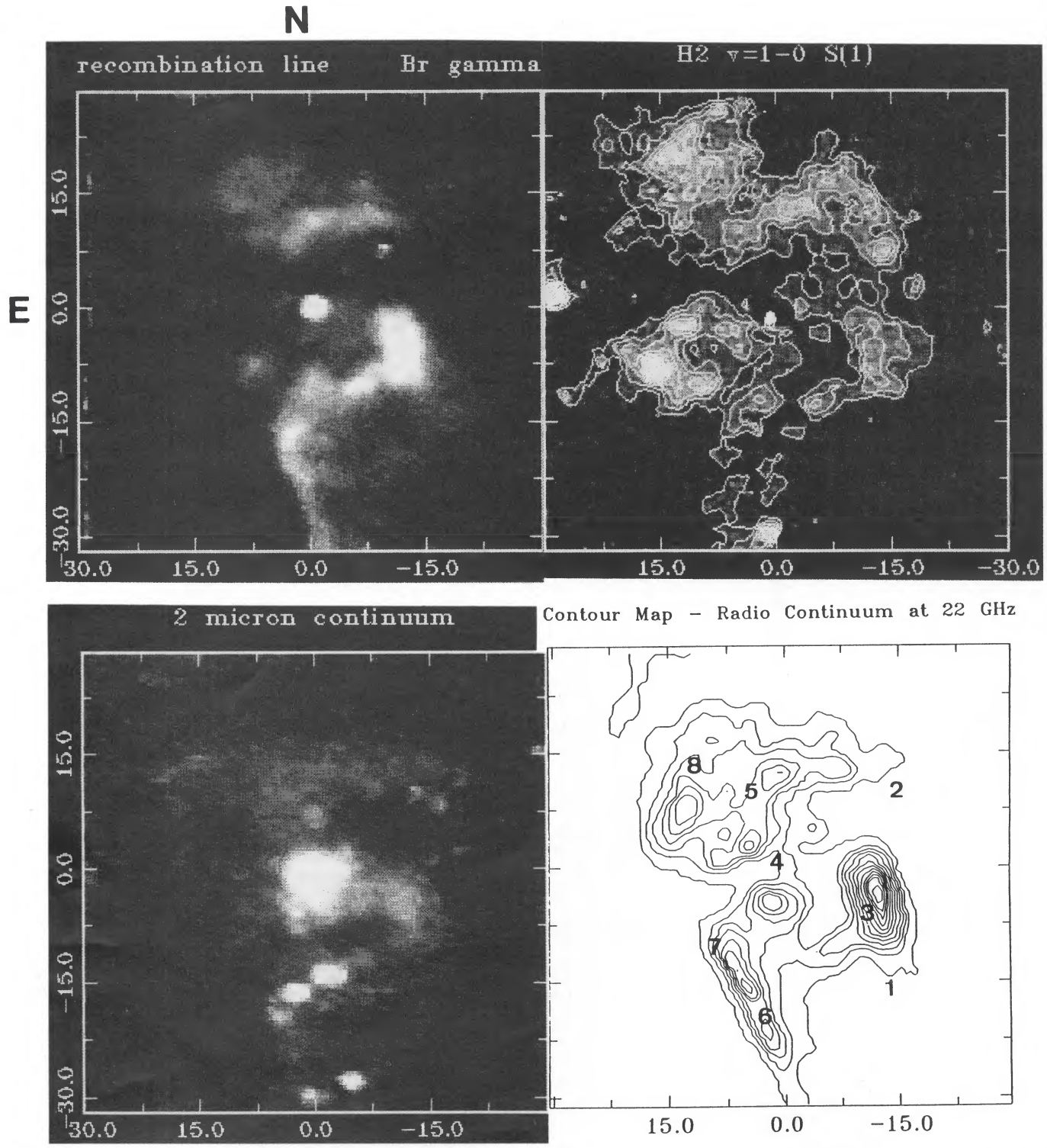

FIG. 1.—Positional offsets are in arcseconds relative to S106IR at $\alpha = 20^h25^m33^s.8$, $\delta = +37°12'50''$ (epoch 1950). North is up and east is left. (*top left*) The distribution of Brγ emission ($\lambda = 2.166$ μm). The gray-scale representation ranges between 2×10^{-11} and 2×10^{-10} W cm^{-2} sr^{-1}. (*top right*) An image in the $v = 1$–0 $S(1)$ transition of H_2 emission ($\lambda = 2.122$ μm). The gray scale ranges between 6×10^{-13} and 2×10^{-11} W cm^{-2} sr^{-1}. Contours are for a running means of 3×3 pixels, with an interval of 2×10^{-12} W cm^{-2} sr^{-1} above a level of 6×10^{-12} W cm^{-2} sr^{-1}. (*Bottom left*) An image of the 2 μm continuum containing *off-line* data for top left frame. The contour interval is linear. (*Bottom right*) Radio continuum emission at 22 GHz reproduced from Felli *et al.* (1984). The contours are linear in 8% steps starting at 4% of the peak flux, corresponding to steps of 0.153 Jy per beam. The 20 μm sources detected by Gehrz *et al.* (1982) are also shown together with their numbers.

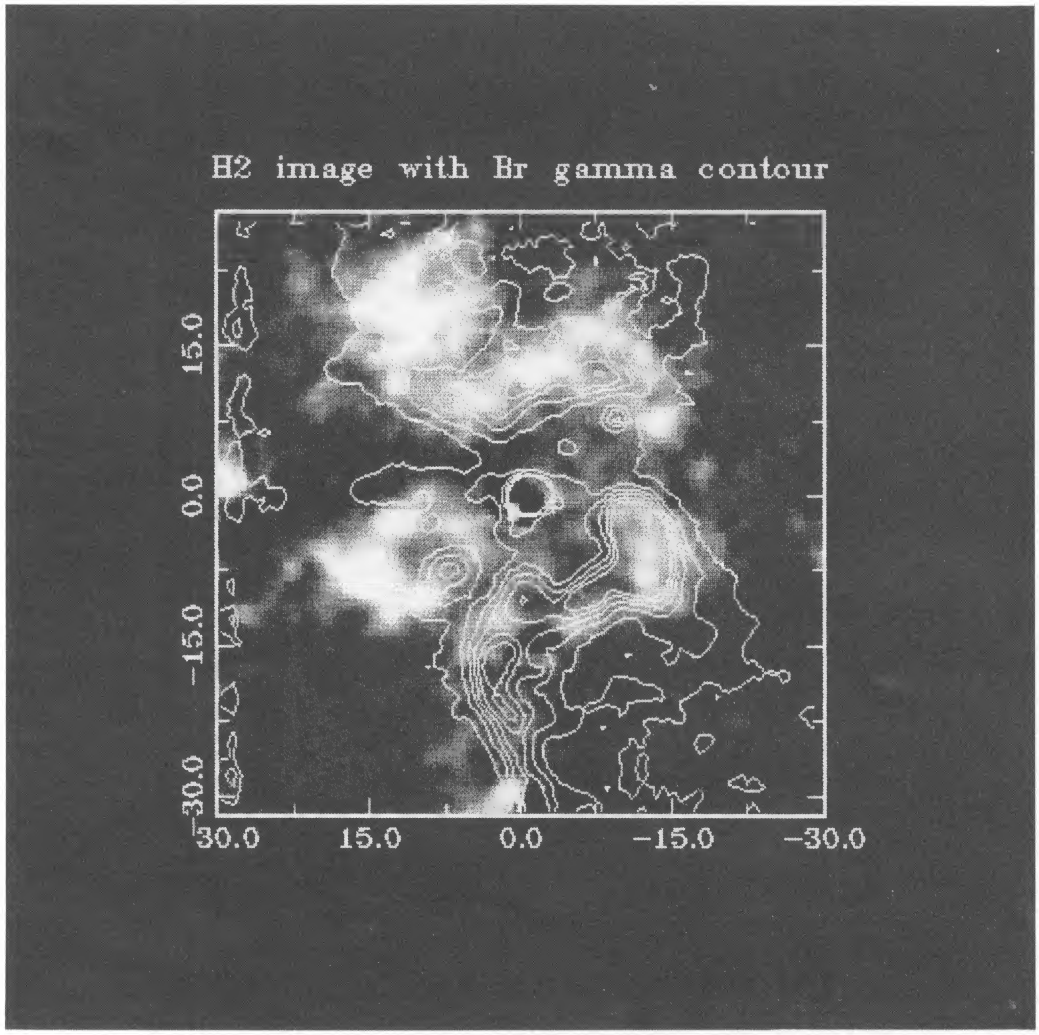

FIG. 2.—Brγ contours overlaid on the H_2 image. Both data sets are smoothed to 3 × 3 pixels. H_2 image displayed in the range 1×10^{-12} to 2×10^{-11} W cm^{-2} sr^{-1}, and Brγ contours spaced by 4×10^{-11} W cm^{-2} sr^{-1} above a level of 1×10^{-12}. Note the displacement between the peaks of the two species; the H_2 emission is shifted farther from S106IR than the adjacent ionized ridges.

HAYASHI *et al.* (*see* **354**, 243)

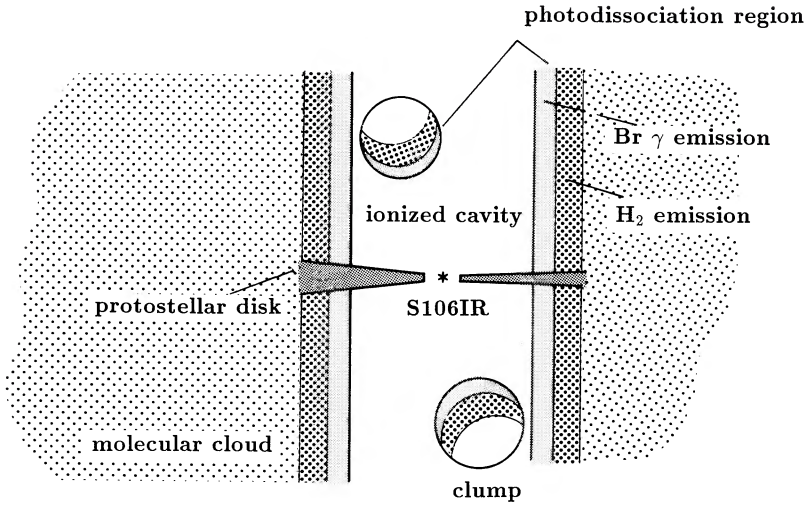

FIG. 3.—Schematic picture of the S106 region showing a cross section of the H II region, the H_2 emission region, and the ambient molecular cloud

geometry of the vibrationally excited molecular hydrogen and the ionized gas in S106 is sketched in Figure 3.

It has already been shown (Longmore, Robson, and Jameson 1986) that all the observed H_2 emission could be produced either by shock excitation or by fluorescence by UV radiation from S106IR. In the latter case, the observations can be understood in terms of a model of photodissociation regions (e.g., Tielens and Hollenbach 1985), in which the surface of a dense molecular cloud is illuminated by an intense far-ultraviolet radiation field. The nonionizing UV photons penetrate the ionization front into the neutral gas and excite H_2 molecules via the absorption in the Lyman and Werner bands (912–1108 Å). A tenth of the excited H_2 molecules dissociate, while the rest return to the electronic ground state with vibrational excitation and then cascade down by infrared fluorescence.

Theories of the fluorescent molecular hydrogen have shown that when the predissociation density is low [$n(H_2) \leq 10^4$ cm^{-3}], the level population distribution of fluorescent H_2, and thus the line intensity ratios, are insensitive to the physical parameters of the photodissociation region. That is, the line ratios in this case do not depend on the incident UV flux, the predissociation density, or the temperature (e.g., Black and van Dishoeck 1987; Takayanagi, Sakimoto, and Onda 1987; Sternberg 1988). The case of higher predissociation density has recently been considered (Hollenbach 1988; Sternberg and Dalgarno 1989). When $n(H_2) \geq 10^5$ cm^{-3}, collisional de-excitation in the photodissociation region thermalizes the population in the lower vibrational levels of molecular hydrogen at a gas temperature of $\sim$1000 K, and so the infrared line ratios no longer adopt the values characteristic of fluorescence in the low-density case. Observationally, it becomes difficult to distinguish high-density radiative excitation from thermal excitation in shocks.

In Paper III, Tanaka *et al.* made sensitive measurements of six transitions of H_2 which originate from the energy levels 6471–13,890 K above the ground state. By adopting the theoretical level population distribution for *low-density* fluorescence as a template, they decomposed the observed H_2 emission into *fluorescent* and *thermal* components. For the case of S106, the results show that about 65% of the $v = 1$–0 $S(1)$ emission comes from thermally excited H_2 at an excitation temperature less than 1400 K and that the rest arises from *low-density* fluorescence (see Table 2 in Paper III).

Millimeter-wave observations of molecular lines have shown that the average density of the molecular cloud surrounding S106 H II region is $n(H_2) \simeq 10^4$ cm^{-3} (e.g., Lucas *et al.* 1978; Churchwell and Bieging 1982; Bally and Scoville 1982; Kaifu and Hayashi 1987). In this molecular cloud, however, there are clumps of higher density, as evidenced by the detection of the $J = 5$–4 and the $J = 7$–6 lines of CS (Hayashi *et al.* 1990) and these clumps are entangled with the expanding H II region.

The identification of the *fluorescent* component of S106 with the low-density [$n(H_2) \leq 10^4$ cm^{-3}] photodissociation regions surrounding the H II region seems secure. For the *thermal* component, however, there are two potential origins: collisional de-excitation of fluorescent H_2 (*high-density fluorescence*) or excitation in shocks driven by the expansion of the H II region and the outflow from the protostar. The excitation temperature for the *thermal* component derived in Paper III ($T_{ex} \leq 1400$ K) is lower than the temperature derived for a typical shock-excited source (e.g., $T_{ex} = 2000$ K in Orion-KL; Paper II, and references therein), but is in the range predicted for high-density radiative excitation. In what follows, we examine the relative importance of these two mechanisms with the new, high-spatial resolution images in hand.

First we examine the shock explanation. The reason that shock temperatures are usually measured to be $\sim$2000 K is probably due to the fact that moderate-speed shocks produce a cooling zone in which the ratios of lines emitted are independent of shock speed. This mimics a 2000 K gas if the temperature is inferred from a pair of 2 μm H_2 lines. Since faster shocks are brighter, there is a strong selection effect at work. On the other hand, shocks slower than 10 km s^{-1} do not create hot enough gas for the mechanism to work. As the shock speed is reduced, the temperature derived from any pair of lines tends toward the maximum temperature behind the shock. The surface brightness also drops with shock speed, quite dramatically for the higher excitation lines.

If there are shocks in S106, they must be driven either by the pressure of the H II region, or by the wind from S106IR. It is difficult for H II gas with a sound speed of 10 km s^{-1} to produce shock speeds of more than a few km s^{-1}. Based on the optical spectroscopy, Solf and Carsenty (1982) suggested that

the expansion velocity of the toroid surrounding the protostar is 6 km s^{-1}. The molecular line at highly excited states imply that the dynamical shock, if there is any, will not exceed 10 km s^{-1} (Harris *et al.* 1987). The speed of the cloud concerned here is the expansion, or transverse velocity with respect to the bipolar cavity/outflow, and it is presumably much slower than the *outflow* velocity along the axis of the bipolar lobes (otherwise the shape of the cavity would have been different). This motion is also imposed by the wind from S106IR (e.g., Garden and Geballe 1986). In any event, these measurements imply that the shock speed is of comparable magnitude as the expansion velocity, say 6–10 km s^{-1}. The shock will have propagated at a speed ahead of the ionization front equal to the shock speed divided by the compression ratio in the shock, which will be of order 10. In these circumstances, a 10 km s^{-1} shock will have propagated 3×10^{16} cm in $\sim 10^4$ yr. This represents the separation between the Brγ and H_2 peaks. A calculation of a 7 km s^{-1} shock propagating into an initial density of 10^5 cm^{-3}, and with a cooling function including H_2 dissociation, H_2 line emission, and CO line emission gives the following result. The surface brightness is 10^{-4} ergs s^{-1} sr^{-1}, which is the observed value. The temperature inferred from the 1–0 $S(1)$ and 2–1 $S(1)$ lines of H_2 is 1200 K (Brand 1990). This calculation seems to be consistent with the observation of the H_2 clumps. However, the model is very sensitive to small changes. A decrease of 2 km s^{-1} in the shock speed reduces the surface brightness by a factor of 17. An increase by the same amount raises the apparent temperature to over 1700 K. One favorable note is that the required velocity falls in the velocity range observed in the ionized gas, as referred to above. In summary of this exercise, a slow shock can be one of the feasible explanations for the thermal H_2 emission in S106.

Now we turn to the high-density fluorescence explanation. We first estimate the density in the photodissociation regions toward the peaks of the H_2 emission assuming that the excitation is radiative. As the Brγ peaks delineate the ionization fronts, the displacement of 3″–7″ ($2.7–6.1 \times 10^{16}$ cm) between the Brγ and the adjacent H_2 peaks is a measure of the depth of the H_2 emitting zone from the ionization front. If we take $A_v \simeq 2$ mag for the extinction between the ionization front and the H_2 emitting region (Tielens and Hollenbach 1985), the total hydrogen density of the photodissociation region is estimated as $n(\text{total}) \simeq 10^5$ cm^{-3} [the relation between A_v and $N(H_2)$ is adopted from Dickman 1978]. Therefore, it is self-consistent to assume that the H_2 emission is fluorescent in these peaks, for the deduced density is high enough to thermalize the level populations. The resultant thermal gas temperature is predicted to be ~ 1000 K (Sternberg and Dalgarno 1989). A correspondingly low temperature for the thermal component in S106 has been deduced in Paper III.

The present high-resolution image resolves the H_2 peaks for the first time and gives a good measure of the surface brightness. The peak brightness of the H_2 $v = 1–0$ $S(1)$ emission clumps is $(1–2) \times 10^{-4}$ ergs s^{-1} cm^{-2} sr^{-1} with a clump-interclump contrast of 5 : 1 to 10 : 1. Sternberg and Dalgarno (1989) calculated the surface brightness of the fluorescent H_2 emission for a grid of the intensity of the incident UV radiation and the density in the photodissociation region. The UV radiation field incident upon the ionization front in S106 is estimated as $\sim 10^4$ times stronger than the general background. For this radiation field, the observed surface brightness can be reproduced, within an uncertainty caused by various possible geometries of the emitting zone, if the density is $n(\text{total}) \geq 10^5$ cm^{-3} in the clumps and $n(\text{total}) \simeq 10^4$ cm^{-3} between clumps. These densities agree with the estimates from the millimeter-wave observations.

In conclusion, the high density in the photodissociation region in S106 [$n(\text{total}) \simeq 10^5$ cm^{-3}] estimated from the present H_2 image suggests either that the *high-density fluorescence* is the major origin for the *thermal* component revealed by Paper III, or that this component is produced by *low-velocity shocks*. It is this component which comprises the emission in the bright clumps visible on the H_2 image. In the present model, the *fluorescent* component identified in Paper III arises naturally from the less dense [$n(\text{total}) \simeq 10^4$ cm^{-3}] portions of the neutral envelope around S106.

T. H., M. T., P. W. J. L. B., and I. G. are Visiting Astronomers at the United Kingdom Infrared Telescope, which is operated by the Royal Observatory Edinburgh on behalf of the Science and Engineering Research Council of the United Kingdom. The authors thank Mark Casali and Tom Geballe for their help during this experiment, and Professor Norio Kaifu for the promotion of the international collaboration which produced this paper. Suggestions from an anonymous referee were instructive and helped to improve this paper. T. H. and M. T. were supported by the Japanese Society for the Promotion of Science.

REFERENCES

Aspin, C., McLean, I. S., Rayner, J. T., and McCaughrean, M. J. 1988, *Astr. Ap.*, **197**, 242.
Aspin, C., McLean, I. S., Schwarz, H. E., and McCaughrean, M. J. 1989*a*, *Astr. Ap.*, in press.
Aspin, C., Rayner, J. T., McLean, I. S., and Hayashi, S. S. 1989*b*, *M.N.R.A.S.*, submitted.
Bally, J., and Scoville, N. Z. 1982, *Ap. J.*, **255**, 407.
Bally, J., Snell, R. L., and Predmore, R. 1983, *Ap. J.*, **272**, 154.
Beckwith, S., Persson, S. E., Neugebauer, G., and Becklin, E. E. 1978, *Ap. J.*, **223**, 464.
Bieging, J. H. 1984, *Ap. J.*, **286**, 591.
Black, J., and van Dishoeck, E. 1987, *Ap. J.*, **322**, 412.
Brand, P. W. J. L. 1990, in preparation.
Churchwell, E., and Bieging, J. H. 1982, *Ap. J.*, **258**, 515.
Dickman, R. L. 1978, *Ap. J. Suppl.*, **37**, 407.
Felli, M., Staude, H. J., Reddmann, T., Massi, M., Eiroa, C., Hefele, H., Neckel, T., and Panagia, N. 1984, *Astr. Ap.*, **135**, 261.
Gatley, I., *et al.* 1987, *Ap. J. (Letters)*, **318**, L73 (Paper I).
Garden, R. P., and Geballe, T. R. 1986, *M.N.R.A.S.*, **220**, 611.
Gehrz, R. D., Grasdalen, G. L., Castelaz, M., Gullixson, C., Mozurkewich, D., and Hackwell, J. A. 1982, *Ap. J.*, **254**, 550.
Harris, A. I., Stutzki, J. R., Lugten, J. B., Stacey, G. J., and Jaffe, D. T. 1987, *Ap. J. (Letters)*, **322**, L49.
Harvey, P. M., Gatley, I., Thronson, H. A., Jr., and Werner, M. W. 1982, *Ap. J.*, **258**, 568.
Harvey, P. M., Lester, D. F., and Joy, M. 1987, *Ap. J. (Letters)*, **316**, L75.
Hasegawa, T., Gatley, I., Garden, R. P., Brand, P. W. J. L., Ohishi, M., Hayashi, M., and Kaifu, N. 1987, *Ap. J. (Letters)*, **318**, L77 (Paper II).
Hayashi, M., Hasegawa, T., Gatley, I., Garden, R., and Kaifu, N. 1985, *M.N.R.A.S.*, **215**, 31P.
Hayashi, S. S., *et al.* 1990, in preparation.
Hodapp, K.-W., and Becklin, E. E. 1988, cited in Gatley, I. 1988, *Science*, **242**, 1264.
Hollenbach, D. J. 1988, *Ap. Letters Comm.*, **26**, 191.
Kaifu, N., and Hayashi, S. S. 1987, in *IAU Symposium 115, Star Forming Regions*, ed. M. Peimbert and J. Jugaku (Dordrecht: Reidel), p. 369.
Longmore, A. J., Robson, E. I., and Jameson, R. F. 1986, *M.N.R.A.S.*, **221**, 589.
Lucas, R., Le Sequeren, A. M., Kazes, I., and Encrenaz, P. J. 1978, *Astr. Ap.*, **66**, 155.
McLean, I. S. 1989, in *Proc. 3d NASA Ames Workshop on IR Detectors*, ed. C. McCreight, in press.
McLean, I. S., *et al.* 1987, *M.N.R.A.S.*, **225**, 393.
McLean, I. S., Chuter, T. C., McCaughrean, M. J., and Rayner, J. T. 1986, *Proc. SPIE*, **627**, 430.
Merrill, K. M., Soifer, B. T., and Russell, R. W. 1975, *Ap. J. (Letters)*, **200**, L37.
Mezger, P. G., Chini, R., Kreysa, E., and Wink, J. 1987, *Astr. Ap.*, **182**, 127.

Persson, S. E., Geballe, T. R., McGregor, P. J., Edwards, S., and Londsdale, C. J. 1984, *Ap. J.*, **286**, 289.
Sellgren, K., Werner, M. W., and Dinerstein, H. L. 1983, *Ap. J. (Letters)*, **271**, L13.
Smith, H. A., Larson, H. P., and Fink, U. 1981, *Ap. J.*, **244**, 835.
Solf, J., and Carsenty, U. 1982, *Astr. Ap.*, **113**, 142.
Staude, H. J., Lenzen, R., Dyck, H. M., and Schmidt, G. D. 1982, *Ap. J.*, **255**, 95.
Sternberg, A. 1988, *Ap. J.*, **332**, 400.
Sternberg, A., and Dalgarno, A. 1989, *Ap. J.*, **338**, 197.
Takayanagi, K., Sakimoto, K., and Onda, K. 1987, *Ap. J. (Letters)*, **318**, L81.
Tanaka, M., Hasegawa, T., Hayashi, S. S., Brand, P. W. J. L., and Gatley, I. 1989, *Ap. J.*, **336**, 207 (Paper III).
Tielens, A. G. G. M., and Hollenbach, D. 1985, *Ap. J.*, **291**, 722.

COLIN ASPIN and SAEKO S. HAYASHI: Joint Astronomy Centre, 665 Komohana Street, Hilo, HI 96720

PETER W. J. L. BRAND: Department of Astronomy, University of Edinburgh, Royal Observatory, Edinburgh, EH9 3HJ, Scotland, UK

IAN GATLEY: National Optical Astronomy Observatories, 950 North Cherry Avenue, P.O. Box 26732, Tucson, AZ 85726-6732

TETSUO HASEGAWA and MASUO TANAKA: Institute of Astronomy, University of Tokyo, Osawa, Mitaka, Tokyo 181, Japan

MASAHIKO HAYASHI: Department of Astronomy, University of Tokyo, Yayoi, Bunkyo, Tokyo 113, Japan

IAN S. MCLEAN: Department of Astronomy, University of California at Los Angeles, 405 Hilgard Avenue, Los Angeles, CA 90024